Check for updates

Novel cytokine-loaded PCL-PEG scaffold composites for spinal cord injury repair

Pangbo Wang, [ID] [a] Hufei Wang,[b] Kang Ma,[a] Shi Wang,[a] Chuanyan Yang,[a] Ning Mu,[a] Fei Yang, [ID] *[b] Hua Feng*[a] and Tunan Chen*[a]

Severe spinal cord injury (SCI) always leads to permanent sensory and motor dysfunction. However, the therapeutic effects of current treatment methods, including high dose methylprednisolone, surgical interventions and rehabilitative care, are far from satisfactory. In recent years, cellular, molecular, tissue engineering and rehabilitative training have shown promising results in animal models. Poly-ε-caprolacton (PCL) – based hydrogel composite system has been considered as a promising strategy to direct the axon growth and mimic the properties of natural extracellular matrix. In this study, we found the addition of the fibroblast growth factor 2 (FGF2) and epidermal growth factor (EGF) to the hydrogel induces the production of axon growth-supportive substrates. The addition of the glial-derived neurotrophic factor (GDNF) to the hydrogel further induces axon directional growth. This "five-in-one" composite scaffold, referred to as PCL/PEG/FGF2/EGF/GDNF, improved the locomotor function in rats 8 weeks after spinal cord injury (SCI) after implantation in transected spinal cord. Furthermore, histological assessment indicated that the designed composite scaffold guided the neuronal regeneration and promoted the production of axon growth-supportive substrates, providing a favorable biological microenvironment. Our novel composite scaffold provides a promising therapeutic method for SCI.

1. Introduction

Spinal cord injury (SCI) is a serious public health problem. There are approximately 180 000 new cases recorded worldwide each year,[1] and the direct cost per injured patient is reported to be about 1–4 million dollars over a lifetime,[2] not to mention the suffering of severe sensory, motor and autonomic nervous dysfunction. Once triggered by an external physical impact,[3] a series of complex pathological changes will occur around the injury, which may seriously hinder axonal regeneration and functional recovery. These pathological changes include ischemia, glial and neuronal necrosis, and immune cell infiltration in the acute and subacute phases,[4] glial scars, cystic cavity formation, lack of neurotrophic stimulation or permissive substrates[5] in the chronic phase. Over the past century, progress in SCI mechanism research has promoted the development of clinical management. The use of the high dose methylprednisolone, surgical interventions and rehabilitative protocols have decreased the morbidity and improved the functional outcomes of SCI patients.[6,7] Despite all this, the curative effect is far from satisfactory. Especially in the repair of injured spinal cord, there is still no good strategy.

Neuroprotective and neuroregenerative therapies have been translated from preclinical studies into clinical trials.[8] However, no randomized clinical trial has demonstrated the efficacy of a repair strategy for improving functional recovery from SCI at present.[6] and recent advances in biological and engineering strategies have provided us with a promising alternative. Considering the complicated pathological condition, a comprehensive treatment based on the pathophysiological mechanism seems to be more effective.

Previous studies have demonstrated that both growth-supportive substrate and chemoattraction, barely expressed in adults, are essential factors for axon growth.[9] Adding fibroblast growth factor 2 (FGF2)[10] and epidermal growth factor (EGF)[11] into the hydrogel could increase axon growth-supportive substrates, such as laminin.[9,12] And increasing glial-derived growth factor (GDNF) could chemoattract and promote pro-priospinal axonal regeneration.[13–15] Although these measures seem promising, the injury site is always replaced by fluid-filled cysts in chronic SCI. Thus, some mechanical substrates that provide physical support for axonal regeneration and the cytoarchitectural organization required for nerve regrowth is very essential.[16]

Therefore, an ideal strategy is to provide a suitable level of architecture, which could be used in regenerative medicine,[17] including slow delivery of cytokines, and the ability to replicate.[18] We focus on the goals of anatomical and functional reconstruction in chronic SCI.

[a]Department of Neurosurgery, Southwest Hospital, Third Military Medical University (Army Medical University), Chongqing 400038, China. E-mail: ctn_666@sina.com
[b]Beijing National Laboratory for Molecular Sciences, State Key Laboratory of Polymer Physics & Chemistry, Institute of Chemistry Chinese Academy of Sciences, Beijing, 100190, China

Poly-ε-caprolacton (PCL) is a biocompatible copolymer, which is widely used in biomaterials and various devices.[19,20] Hydrogels, highly hydrated materials, have emerged as suitable biomaterials to replace the extracellular matrix (ECM) for modeling cellular microenvironments.[21–24] Here, a combined strategy involving the construction of hydrogels and cytokines in the PCL hybrid fibers was reported. The aim of those measures is to establish an ecological microenvironment that could provide directional guidance for axonal regeneration while supplying simulated extracellular environment, including cytokines and mechanical compliance.

As illustrated in Fig. 1, we started with the construction of the composite hydrogel cytokine PCL scaffold with a guide conduit. Combined with the function of sustainable release of the growth factor, the composite scaffolds are expected to provide favorable environment for promoting directional growth and regeneration of axons. According to the presence of PCL or not, these composites are divided into two groups and transplanted into the transected SCI model.

2. Results and discussion

2.1. Construction and characteristics of the composite scaffolds

Poly-ε-caprolacton (PCL) was used as the framework of hydrogels due to its stability, biocompatibility and directional guidance in the tissue. It was prepared successfully showed by electrospinning technology (Fig. 2A). The dimensional size of the PCL was 200 ± 10 μm, as determined using a scanning electron microscope. Nuclear magnetic spectroscopy and infrared spectroscopy were used to identify them (Fig. 2B and C). The slow release characteristics of the PEG hydrogels has been reported in previous reports.[25–27] The PCL electrospinning was evenly placed in a special mold with a gap in the middle, and then the hydrogel was evenly filled around the PCL. The diameter of the scaffold complex was controlled at about 3.5 mm, which was close to the diameter of the rat spinal cord. BET surface area, pore volume and pore diameter of the hydrogel Pec-g-PHEAA was found to be 7.7254 m^2 g^{-1}, 7.7254 m^2 g^{-1} and 16.66 Å, respectively. As shown in the Prajwal's research, hydrogels with similar BET surface area physical properties exhibited good adsorption capabilities.[28] The porous morphology facilitates the transport of nutrients and provides suitable scaffold to support cell growth and survival.[29] To construct PCL/PEG/FGF2/EGF/GDNF composites, the PEG hydrogels containing FGF2, EGF and GDNF were infiltrated into the PCL network before solidification (Fig. 2E and F). As illustrated in Fig. 3A, PCL-PEG scaffold composite has excellent sustained-release effect on FGF2, EGF and GDNF. When the experiments were processed to 21 days, the cumulative release amount was close to 25%. The sustained and slow release of these cytokines was beneficial to stimulate surrounding cells to secrete substrates that support the growth of neuron axons and to further chemically induce axons. As shown in Fig. 3B–D, although the compressive modulus of PCL-PEG scaffold (range at 0.83–2.4 kPa) composites was significantly higher than that of PEG hydrogels (range at 2.75–5 kPa), they also met the mechanical requirement of the normal spinal cord tissue.[30,31]

2.2. Morphology distribution of neurites on the composites

PC12 cells were cultured on the composites to analyze its effect on cell viability and neurite growth. CCK8 assay illustrated that there was no significant difference between the PCL group and the control group about the absorbance at 450 nm (Fig. 3E). Florescence images of the cells cultured on composites were shown in Fig. 4. Compared with the control group (Fig. 4D–F), pure PCL could promote neurites adhesion and directional growth (Fig. 4A–C). FGF2, EGF and GDNF were not added to the medium because their roles were already clear.[10,11,14,15] In addition, we quantified directional growth cells in different groups. We found that as shown in Fig. 3F, the number of directional growth cells in the PCL group was significantly higher than that in the control group.

2.3. Composite scaffold promotes anatomical and functional recovery of SCI rats

As shown in Fig. 5A, rat spinal cords were transected, and different implants were placed in the defect site through microsurgery. The operated rats were divided into three groups to receive different implants: group 1, control group with only PBS injection; group 2, PEG + FGF2 + EGF + GDNF; group 3, PCL + PEG + FGF2 + EGF + GDNF. Behavioral analyses were performed to evaluate the hind limb locomotion of the rats every week after SCI by the Basso, Beattie, and Bresnahan (BBB) scale.[32] Initial BBB scores of all rats after SCI were close to 0 and subsequently showed different degrees of rehabilitation. From the 7 weeks after SCI, BBB score of group 3 was significantly higher than that of group 1 and 2. The BBB score of group 3 reached a level of 7–8, suggesting a locomotion recovery of rats after SCI (Fig. 5B).

Subsequently, all rats were sacrificed to assess the histological evidence of neuronal regeneration 8 weeks after SCI (as shown in Fig. 5C). In the histological specimen, we observed that the body surrounding the scaffold composite was filled with tissues, and its shape did not change significantly. We concluded that the stability of the hydrogel meets our needs for spinal cord repair.
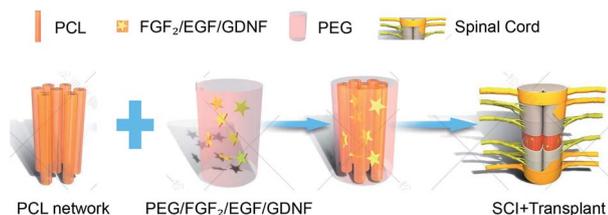

Fig. 1 Design of a cytokine-containing hydrogel embedded in a PCL scaffold composite, and schematic representation of implantation into the spinal cord.
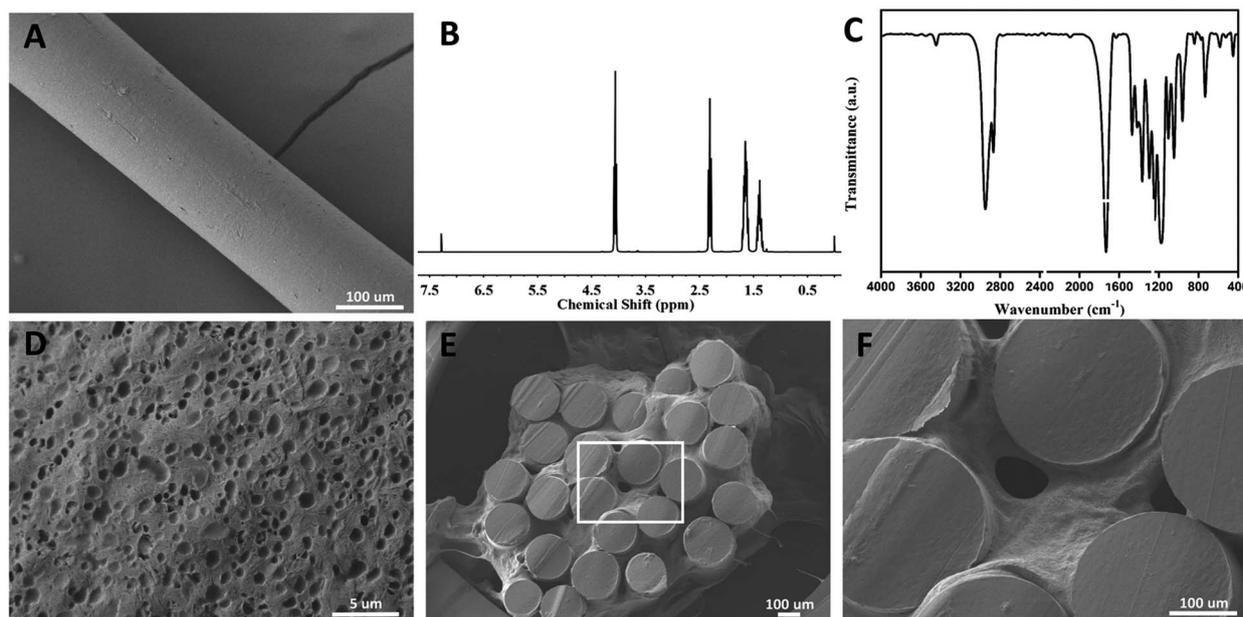
Fig. 2 The physical characterizations of cytokine-loaded PCL-PEG scaffold composite. (A) A representative scanning electron microscopy (SEM) image of PCL; (B and C) analysis of PCL by infrared spectrum (IR) and nuclear magnetic resonance spectroscopy (NMR); (D and E) a representative scanning electron microscopy (SEM) image of PEG and cytokine-loaded PCL-PEG scaffold composite; (F) enlarged view of the scaffold composite.

2.4. Histological evaluation of composite scaffold promoting axon regeneration

Immunofluorescence staining and hematoxylin and eosin (H&E) staining were performed to observe tissue bridging and neuronal axon regeneration (Fig. 6A–C). As showed in H&E staining, the tissue was discontinuous, and even cavities appeared in some places of group 1 and 2. By contrast, the tissue around injury site of the group 3 was orderly organized
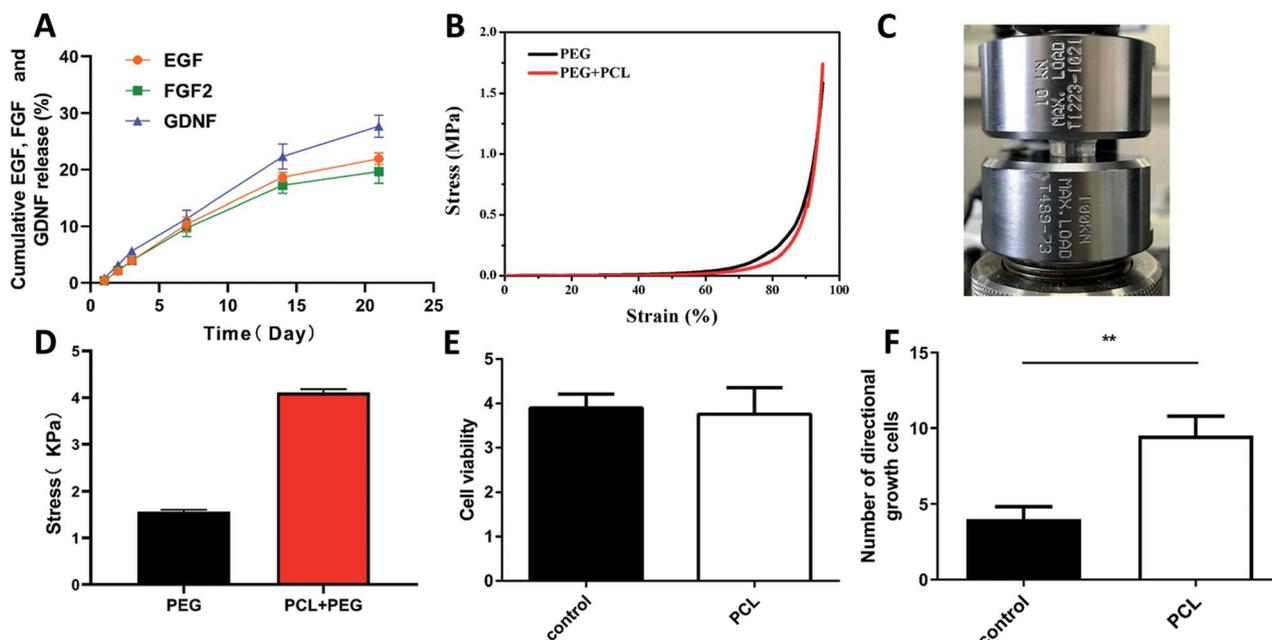

Fig. 3 Slow-release, mechanical, and biocompatibility of cytokine-loaded PCL-PEG scaffold composite. (A) the cumulative release of EGF, FGF2 and GDNF from the PEG hydrogels, as determined by the ELISA kits; (B–D) the cyclic compression stress−strain curves of PEG hydrogels and PCL-PEG scaffold composite and the comparison between them; (E) bar graph showing the proliferation of PC12 cells with PCL co-culture or not by using CCK8 assay on day 3 ($n = 6$); (F) comparison of the number of directional adhesion cells between the two groups. *$P < 0.05$, **$P <$ 0.01, One-Way ANOVA followed by Tukey's *post hoc* test. N. S. indicates no significant difference.
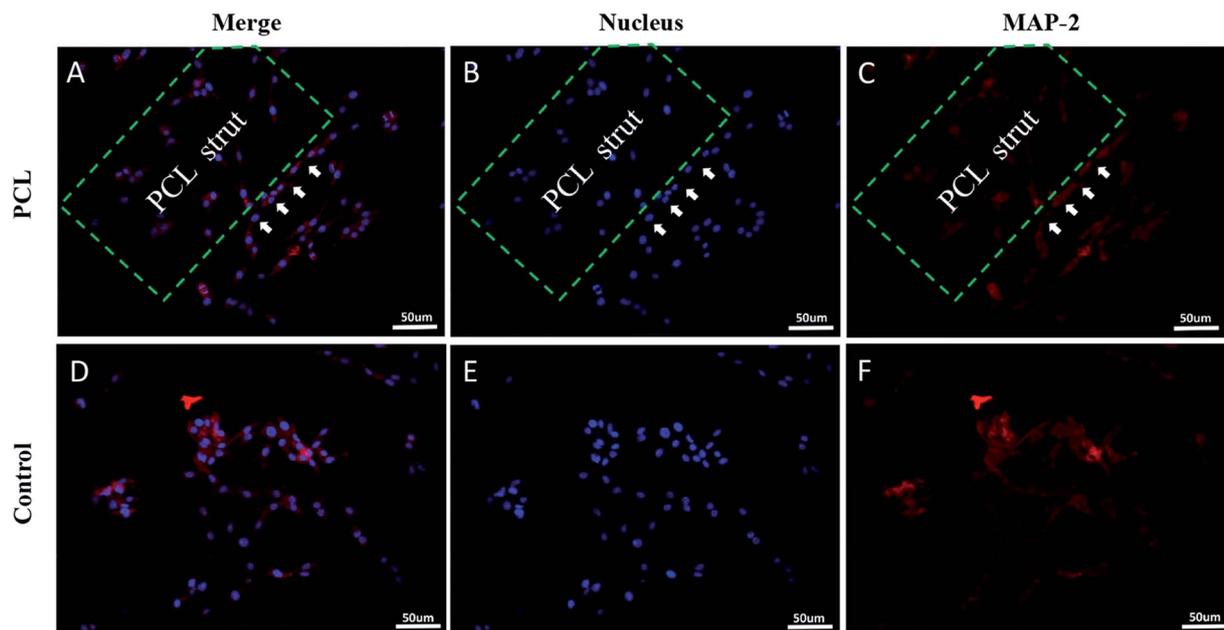
Fig. 4 Fluorescence staining of PC12 cells after being cultured with the PCL for 3d indicated that PC12 cells grow directionally along PCL (A−C). The PC12 cells in the control group were relatively disorganized (D−F). DAPI (blue, a cell nucleus marker), and MAP2 (red, a neuronal marker).

and filled around the composite scaffold. Immunofluorescence staining demonstrated that there were few neurons (MAP2-positive cells, green) in the injury sites of group 1 and 2. In contrast, more MAP2-positive neurons appeared at the injury site and showed a directional extension in group 3. However, they did not run through the entire conduit. These phenomena
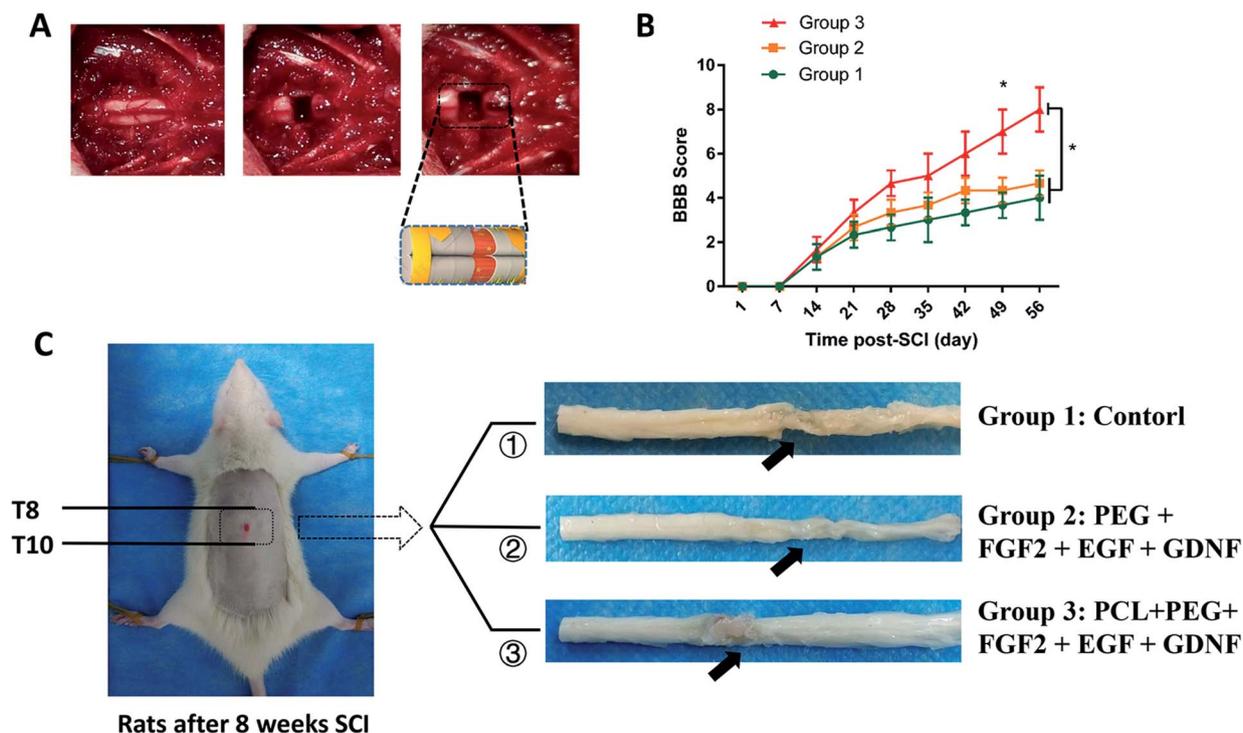

Fig. 5 Scaffold implantation and behavioral evaluation. (A) Establishment of spinal cord transection model and implantation of scaffold composite; (B) BBB scores during a 8 week follow-up, data presented as mean ± standard deviation ($n = 5$ for each group). p values in (B) were determined by one-way analysis of variance (ANOVA) followed by Tukey's *post hoc* test, * denotes $p < 0.05$. (C) The representative spinal cord samples 8 weeks after transplantation; the arrows pointed to the lesion sites.

suggested that the combination of cytokines and PCL produced a better histological effect than only adding the cytokines. Quantitative analysis indicated that the density of regenerated axon in group 3 was significantly higher than that in group 1 and 2 ($p < 0.05$; Fig. 6D).

In addition, as shown in Fig. 7A and B, we evaluated the expression of laminin at the injury site by immunofluorescence. Quantitative analysis indicated that the density of regenerated laminin in group 3 was significantly higher than that in group 1 and 2 ($p < 0.05$; Fig. 7C). And they got a common label with the regenerated axons (Fig. 7D). This was in line with our expectations that the FGF2 and EGF in the PEG hydrogel could promote the expression of the laminin which was the growth-supportive substrates of axon.[33] It was the PCL that provided the scaffold which contributed to the directional guidance.

2.5. Discussion

Although completely transected spinal cord injury (SCI) is rarely seen in human patients, the corresponding animal model can provide accurate information for the study of axonal regeneration. Compared with the completely SCI model, incomplete SCI model, such as compression and contusion injury model, has a large individual heterogeneity. What's more, the sprouting of the surrounding normal spinal cord tissue around the injury site in incomplete SCI model may lead to the recovery of spinal cord function,[34,35] making it is difficult to judge whether the recovery of function was resulted from axon regeneration of the injured neurons or not.[36] In contrast, the complete SCI model does not have any spared axons in the lesion space, so axon regeneration will be clearly identified. Therefore, we chose the T9 complete SCI model to study the repairing effects of our strategy on SCI.
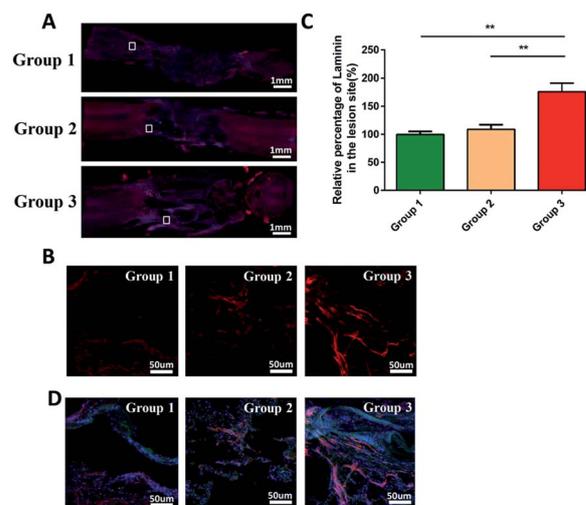

Fig. 7 Immunofluorescence staining to evaluate the production of laminin at the injury site 8 weeks after SCI. (A) Immunofluorenscence staining for the longitudinal sections at low magnification; (B) is an enlarged view of local tissue stained with immunofluorenscence: laminin (red, a supportive substrate marker). (C) Quantification of the percentages of laminin in the lesion area of the rats in each group. Data presented as mean ± standard deviation ($n = 3$ for each group). p values in (C) were determined by one-way analysis of variance (ANOVA) followed by Tukey's *post hoc* test, * denotes $p < 0.05$, ** denotes $p < 0.01$. (D) Immunofluorescence staining images: MAP2 (blue, a neuronal marker), laminin (red, a supportive substrate marker). They are close to each other in position.

Cell transplantation therapy has enormous potential in the repairing damage caused by the non-renewable cells' loss. However, the efficacy and long-term safety of cell
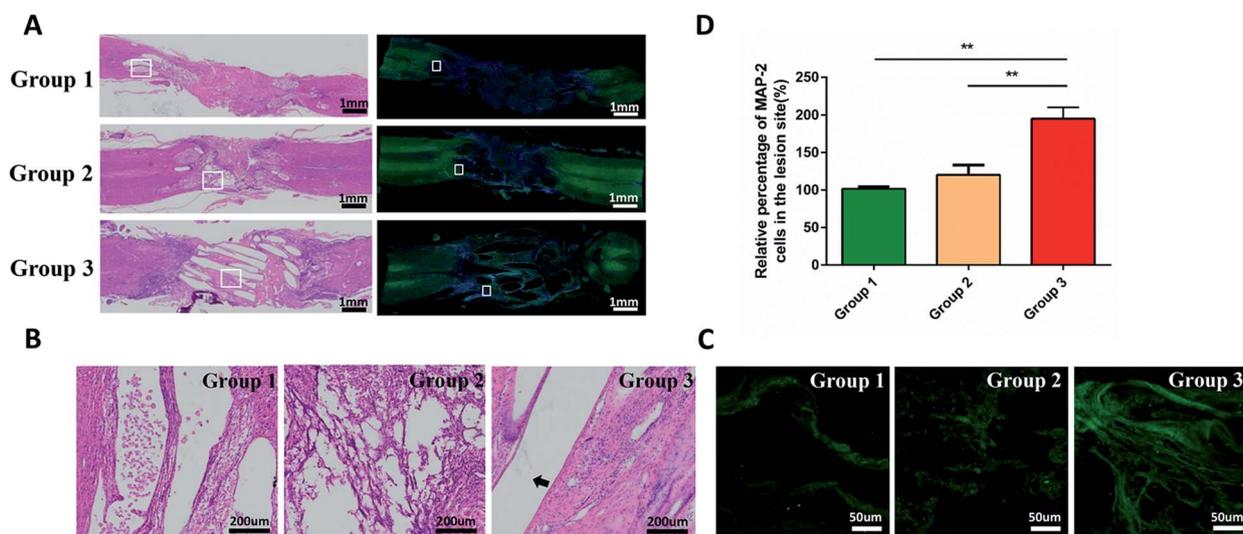

Fig. 6 Histological assessment on the longitudinal sections of the spinal cords at 8 weeks after SCI. (A) H&E (left) and immunofluorenscence (right) staining for the longitudinal sections at low magnification; (B) is an enlarged view of local tissue stained with HE. (C) Is an immunofluorescence staining images: MAP2 (blue, a neuronal marker). The arrows pointed to the PCL. Immunofluorescence showed that axonal regeneration was more pronounced in group 3 and followed the PCL direction. (D) Quantification of the percentages of Tuj-1-positive neurons in the lesion area of the rats in each group. Data presented as mean ± standard deviation ($n = 3$ for each group). p values in (D) were determined by one-way analysis of variance (ANOVA) followed by Tukey's *post hoc* test, * denotes $p < 0.05$, ** denotes $p < 0.01$.

transplantation therapy remain unproven.[37] When these exogenous stem cells are transplanted to the injured spinal cord, how to make sure they survive and differentiate into functional neurons in the harsh microenvironment remains unresolved.[38] Even if these cells survive and differentiate into neurons, how to establish synaptic connections and work with other neurons also need to be addressed. Since little is known about the mechanisms how the transplanted cells promote repair and mediate functional improvements after SCI,[39] we did not choose cell transplantation in this study.

Michael[40] reviewed that long-distance axon regeneration across lesions to reach the original targets was essential for functional recovery of SCI, especially for complete SCI. He also reported that a single intervention was hardly to achieve the repair of SCI, and neuron-intrinsic growth programs, permissive substrates and chemo-attractive molecules were all essential factors in the axon regeneration after SCI. Based on this theory, we selected PCL, a biodegradable and aliphatic polysaccharide, as a multifunctional tools to bridge the lesion gap in order to allow axon growth, create a more favorable endogenous environment combined with the surrounding hydrogels.[41,42] Delivering fibroblast growth factor 2 (FGF2) and epidermal growth factor (EGF) into the hydrogel increased the production of axon growth-supportive substrates, such as laminin.[9] Delivering glial-derived neurotrophic factor (GDNF), which was reacted with GDNFR expressed on the propriospinal axons, into the hydrogel further chemoattractted axon regeneration. As a result, this scaffold composite promoted the directional regeneration of axons along the scaffold composite. Moreover, they also promoted the regeneration of laminin around the axons, and laminin and regenerated axons were co-standardized.

Using this reproducible, readily available scaffold composite effectively promoted axon repairment after SCI. This finding suggested that designing materials from the perspective of pathophysiology might be a feasible direction for tissue engineering in SCI repair.

3. Experimental

3.1. Fabrication of scaffold composite

PCL was prepared *via* electrospinning technology. Before mixed with PEG, the PCL scaffolds were immersed in 75% ethanol for sterilization and then washed by PBS twice. The PCL scaffolds were sterilized in 75% alcohol for at least 30 minutes at room temperature. Then they were washed in sterile PBS at least three times, each time greater than 10 minutes. PEG was prepared as below. Briefly, using a four-arm polyethylene glycol succinimide glutarate (tetra-PEG-SG, relative molecular mass of 10 000) mixed with dopamine and pure water to make A, using tetra-PEG-NH$_2$ (relative molecular mass of 10 000) dissolved in disodium hydrogen phosphate (28 mmol L^{-1}) to make B, A and B were mixed in equal amounts. Then 1.0 µg µL^{-1} of FGF2, EGF, and GDNF were added to the mixture according to the Mark A's protocol,[9] and left it for solidification, or mixed these PEG evenly around the PCL. The entire process remained sterile. Finally, PCL/PEG/FGF2/EGF/GDNF composites and PEG/FGF2/

EGF/GDNF composites were successfully prepared, and they were cut into 2 mm pieces.

3.2. Characteristics of the scaffold composite

After preparation of these composite, nuclear magnetic spectroscopy and infrared spectroscopy were used to identify PCL. Then the microstructure of PCL, PEG and scaffold complexes was observed by scanning electron microscopy.

3.3. Mechanical testing

Mechanical testing of the PEG hydrogels and PCL-PEG scaffold composite was carried out using universal tensile machine. Compression and cyclic compression tests were performed on cylindrical samples with a diameter of 13 mm and a height of 7 mm at a speed of 3 mm min^{-1}. Compress the sample to a compression strain of 20–30%. Each group of hydrogels was tested at least 3 times.

3.4. Brunauer–Emmett–Teller (BET) surface area analysis

After successfully constructing a PEG hydrogel with a diameter of 8 mm and a height of 4 mm, the BET specific surface area of the PEG hydrogel was measured by a fully automatic specific surface area and porosity analyzer (Micromeritics ASAP2460).

3.5. Release kinetics of EGF, FGF2 and GDNF

Procedures for determining EGF, FGF2 and GDNF release kinetics from PCL-PEG scaffold are briefly summarized below in accordance with the previously published technique.[24,43] After successfully constructing a cytokine scaffold composite with a concentration of 1.0 µg µL^{-1} in a 96-well plate, we cut it into an average of about 3 mm. Then, the EGF, FGF2 and GDNF-loaded scaffold composite were incubated with 1 mL tris buffer (20 × 10^{-3} m Tris–HCl, 150 × 10^{-3} m NaCl, 0.1% BSA, pH = 7.4) at 37 °C. At various time points, buffers were taken out and kept at −20 °C before the measurements; in the meanwhile, 1 mL fresh buffer was added. The cumulative release of EGF, FGF2 and GDNF were quantified by ELISA kits (R&D systems). The release efficiency of EGF, FGF2 and GDNF was calculated according to the following formula:

$$\text{Release efficiency (\%)} = [(W_a - W_b)/W_a] \times 100\%$$

where W_a and W_b are the weight of EGF, FGF2 and GDNF in buffers before and after incubation of the cytokine-containing scaffold composite, respectively. The release profiles of EGF, FGF2 and GDNF were obtained by ELISA for 21 successive days.

3.6. Cell experiment

PC12 cells were cultured in RPMI 1640 medium (Gibco, C22400500BT) containing 10 vol% fetal bovine serum (FBS; Gibco, 10099141, USA) in confocal dishes, and then incubated in a humidified atmosphere with 5% CO$_2$ at 37 °C. The culture medium was refreshed every other day.

The PCL was previously fixed on the confocal dishes, and then were immersed in 75% ethanol for sterilization and

washed by PBS and medium twice. PC12 cells were seeded into the culture dishes. After coculturing for 3 days, 20 μL CCK-8 reagent was added to these wells for 60 min at 37 °C. Then the OD value of buffer was measured at 450 nm. The effect of PCL on cell viability was evaluated by the ratio of OD value of PCL group to control group.

Immunofluorescence staining were performed to observe the effect of PCL on PC12 cells' growth. The process was described as below. The samples were fixed using 4 vol% paraformaldehyde for 15 min, and then blocked with 5% v/v fetal bovine serum or with 0.5% v/v Triton-X 100 (Sigma-Aldrich, St. Louis, MO) in PBS. After that, PC12 cells were incubated with chicken polyclonal to microtubule-associated protein-2 (MAP2, 1 : 5000, Abcam, USA) overnight at 4 °C. Then relative fluorescence secondary antibodies were incubated for 1 hour at room temperature. Cell nuclei were stained with 4′-6-diamidino-2-phenylindole (DAPI, Beyotime, Shanghai, China) for 10 minutes at room temperature. Immunofluorescence was examined by confocal microscopy (LSM800, ZEISS, Oberkochen, Germany), and images were obtained using an LSM Image Examiner.

3.7. The spinal cord injury model and the implant seeding

All procedures were approved and performed by the Ethics Committee of Animal Research at the First Affiliated Hospital of Third Military Medical University (Army Medical University), Chongqing. After an initial week of adaptation, female Sprague Dawley rats weighing 180–220 g were modeled. According to Yuan's protocol,[44] the rats were anesthetized with an intraperitoneal injection of 5% chloral hydrate and fixed in the prone position. The laminae of the thoracic vertebrae T8–10 were exposed. Under an operating microscope, the spinal cord was exposed and completely transected along 2 mm at levels T9. The rats immediately showed tail wagging reflex, hind limb and torso retraction and flutter, and subsequent paralysis of the hind limbs, suggesting successful modeling.[45] After adequate hemostasis, the scaffold composites were implanted into the spinal cord gap. Finally, the muscle and skin were sutured with 4–0 nylon sutures.

SCI rats were randomly divided into 3 groups: group 1, blank control group in which the gap was treated with 200 μL PBS injection (n = 8); group 2, the implant group with PEG + FGF2 + EGF + GDNF composites (n = 8); group 3, the implant group with PCL + PEG + FGF2 + EGF + GDNF scaffold composite (n = 8). Every rat received a daily intramuscular injection of penicillin and levofloxacin for 7 consecutive days to prevent infection, and the bladder was emptied every 12 h until the recovery of autonomic urination.

3.8. Basso, Beattie, and Bresnahan locomotor rating scale

The locomotion function of the rat's hind limb was evaluated by the Basso, Beattie, and Bresnahan scale[46] on day 1 after the surgery, and then was repeated once a week until 8 week's implantation. The score ranging from 0 to 21 points was assigned based on conditions such as joint activities, coordinated movement of fore and hind limbs, and trunk and tail

positions. Rats were allowed to crawl freely on a circular platform with a diameter of 2 m, and were observed for at least 5 min by two observers blinded to the study. Five rats from each group were randomly selected for the assessment at each time.

3.9. Histological analysis

Rats were anesthetized with an intraperitoneal injection of overdose 5% chloral hydrate at 8 weeks after the transplantation. Then the rats were perfused with 4% paraformaldehyde. The spinal cord sections within the range of 0.5 cm rostral and caudal to the injury center were removed, dehydrated, embedded, and cryo-sectioned into 5 μm thick slices. H&E staining was performed for general morphology. For immunohistochemistry, after antigen retrieval with citric acid, the sections were sequentially permeabilized in 0.3% Triton X-100 (Sigma, St. Louis, MO) at room temperature for 15 min, blocked in 5% goat serum at 37 °C for 2 h. Then the sections were incubated with primary antibodies overnight at 4 °C, which included polyclonal anti-microtubule-associated protein-2 (MAP2, ab5392, 1 : 5000, Abcam, USA) for regenerated axon and polyclonal anti-laminin (MAB2549, 1 : 200, R&D, USA) for axon growth-supportive substrates. They were incubated with secondary antibodies for 2 h at room temperature: 488-conjugated IgG (Alexa Fluor 488, 1 : 100, Abcam, USA) and 568-conjugated IgG (Alexa Fluor 568, 1 : 100, Abcam, USA). Cell nuclei were stained with 4′-6-diamidino-2-phenylindole (DAPI, Beyotime, Shanghai, China) for 10 minutes at room temperature. Immunofluorescence images were observed by confocal microscopy (LSM800, ZEISS, Oberkochen, Germany), and Virtual Slide Microscope (VS120, Olympus LifeScience, Japan).

To quantify the amount of MAP2 and laminin immunostaining-positive signals, at least three fields per sample (n = 4) were selected, and the Image J software (Wayne Rasband, National Institutes of Health, USA) was used. Then the data were normalized with its value of group 1 (control group = 100%).

3.10. Statistical analysis

The data were analyzed using IBM SPSS Statistics 20 (IBM Corp., Armonk, New York, USA). All data were expressed as mean ± standard error of mean (SEM). Comparisons between means were assessed by a one-way ANOVA and *post hoc* LSD tests for multiple comparisons. A repeated-measures ANOVA was adopted to analyze the data from the same sample at different time points for the behavior assessment. The Student *t* test was used for single comparisons. Percentages were compared *via* the chi-square test or the Fisher exact test when appropriate. $P < 0.05$ was considered statistically significant.

4. Conclusion

In summary, we had successfully constructed a PCL-based hydrogel composite system, in which PCL provided physical support for axonal regeneration, FGF2 and EGF were added to the hydrogel to increase axon growth-supportive substrates (such as laminin), and GDNF was added to further chemoattract

propriospinal axons. The vitro experiments showed that single PCL without FGF2, EGF and GDNF could promote neurites adhesion and directional growth. With the help these cytokines and PEG hydrogels, the PCL-based hydrogel composite system provided a favorable biological microenvironment for cell survival and growth. After implantation in the transected spinal cord tissue, the PCL-based hydrogel composite promoted the axon's directional regeneration in the conduit, thus promoting the recovery of motor function after SCI. Meanwhile, this composite also promoted the production of laminin which played an important role in the axon growth-supportive substrates. These data suggested that PCL-based biomaterials combined with other elements could be a feasible direction for tissue engineering applications.

Ethical statement

This study was performed in strict accordance with the Guide for the Care and Use of Laboratory Animals of NIH (NIH Pub. no. 85-23, revised 1996) and was approved by the Laboratory Animal Welfare and Ethics Committee of the Third Military Medical University and Ethic Committee of Southwest Hospital, Chongqing, China.

Conflicts of interest

There are no conflicts to declare.

Acknowledgements

References

1 M. Fitzharris, R. A. Cripps and B. B. Lee, *Spinal Cord*, 2014, **52**, 117–122.
2 C. S. Ahuja, S. Nori, L. Tetreault, J. Wilson, B. Kwon, J. Harrop, D. Choi and M. G. Fehlings, *Neurosurgery*, 2017, **80**, S9–S22.
3 X. Li, D. Liu, Z. Xiao, Y. Zhao, S. Han, B. Chen and J. Dai, *Biomaterials*, 2019, **197**, 20–31.
4 A. P. Tran, P. M. Warren and J. Silver, *Physiol. Rev.*, 2018, **98**, 881–917.
5 M. B. Bunge, A review journal bringing neurobiology, neurology and psychiatry, *Neuroscientist*, 2001, **7**, 325–339.
6 G. Courtine and M. V. Sofroniew, *Nat. Med.*, 2019, **25**, 898–908.
7 M. G. Fehlings, L. A. Tetreault, J. R. Wilson, B. K. Kwon, A. S. Burns, A. R. Martin, G. Hawryluk and J. S. Harrop, *Global Spine J.*, 2017, **7**, 84S–94S.
8 W. S. El Masri and N. Kumar, *Lancet*, 2011, **377**, 972–974.
9 M. A. Anderson, T. M. O'Shea, J. E. Burda, Y. Ao, S. L. Barlatey, A. M. Bernstein, J. H. Kim, N. D. James, A. Rogers, B. Kato, A. L. Wollenberg, R. Kawaguchi, G. Coppola, C. Wang, T. J. Deming, Z. He, G. Courtine and M. V. Sofroniew, *Nature*, 2018, **561**, 396–400.
10 O. Kashpur, D. LaPointe, S. Ambady, E. F. Ryder and T. Dominko, *BMC Genomics*, 2013, **14**, 656.
11 R. E. White, F. Q. Yin and L. B. Jakeman, *Exp. Neurol.*, 2008, **214**, 10–24.
12 M. A. Anderson, J. E. Burda, Y. Ren, Y. Ao, T. M. O'Shea, R. Kawaguchi, G. Coppola, B. S. Khakh, T. J. Deming and M. V. Sofroniew, *Nature*, 2016, **532**, 195–200.
13 J. R. Siebert, F. A. Middelton and D. J. Stelzner, *BMC Neurosci.*, 2010, **11**, 69.
14 L. X. Deng, P. Deng, Y. Ruan, Z. C. Xu, N. K. Liu, X. Wen, G. M. Smith and X. M. Xu, *J. Neurosci.*, 2013, **33**, 5655–5667.
15 R. B. Campenot, *Proc. Natl. Acad. Sci. U. S. A.*, 1977, **74**, 4516–4519.
16 F. Gelain, S. Panseri, S. Antonini, C. Cunha, M. Donega, J. Lowery, F. Taralli, G. Cerri, M. Montagna, F. Baldissera and A. Vescovi, *ACS Nano*, 2011, **5**, 227–236.
17 F. Gelain, *Int. J. Nanomed.*, 2008, **3**, 415–424.
18 F. Gelain, L. D. Unsworth and S. Zhang, *J. Controlled Release*, 2010, **145**, 231–239.
19 S. M. Loverde, M. L. Klein and D. E. Discher, *Adv. Mater.*, 2012, **24**, 3823–3830.
20 J. M. Miszuk, T. Xu, Q. Yao, F. Fang, J. D. Childs, Z. Hong, J. Tao, H. Fong and H. Sun, *Appl. Mater. Today*, 2018, **10**, 194–202.
21 S. R. Caliari and J. A. Burdick, *Nat. Methods*, 2016, **13**, 405–414.
22 Y. S. Zhang and A. Khademhosseini, *Science*, 2017, **356**, eaaf3627.
23 N. Annabi, A. Tamayol, J. A. Uquillas, M. Akbari, L. E. Bertassoni, C. Cha, G. Camci-Unal, M. R. Dokmeci, N. A. Peppas and A. Khademhosseini, *Adv. Mater.*, 2014, **26**, 85–123.
24 Z. Cai, Y. Gan, C. Bao, W. Wu, X. Wang, Z. Zhang and Q. Zhou, *Adv. Healthcare Mater.*, 2019, **8**, e1900013.
25 F. Q. Hu, Y. Y. Zhang, J. You, H. Yuan and Y. Z. Du, *Mol. Pharmaceutics*, 2012, **9**, 2469–2478.
26 G. Pasut, A. Mero, F. Caboi, S. Scaramuzza, L. Sollai and F. M. Veronese, *Bioconjugate Chem.*, 2008, **19**, 2427–2431.
27 Y. Bae and K. Kataoka, *Adv. Drug Delivery Rev.*, 2009, **61**, 768–784.
28 P. Kulal and V. Badalamoole, *Int. J. Biol. Macromol.*, 2019, DOI: 10.1016/j.ijbiomac.2019.11.181.
29 N. Annabi, J. W. Nichol, X. Zhong, C. Ji, S. Koshy, A. Khademhosseini and F. Dehghani, *Tissue Eng., Part B*, 2010, **16**, 371–383.
30 A. Bakshi, O. Fisher, T. Dagci, B. T. Himes, I. Fischer and A. Lowman, *J. Neurosurg.*, 2004, **1**, 322–329.
31 A. Perets, Y. Baruch, F. Weisbuch, G. Shoshany, G. Neufeld and S. Cohen, *J. Biomed. Mater. Res., Part A*, 2003, **65**, 489–497.
32 Y. D. Teng, E. B. Lavik, X. Qu, K. I. Park, J. Ourednik, D. Zurakowski, R. Langer and E. Y. Snyder, *Proc. Natl. Acad. Sci. U. S. A.*, 2002, **99**, 3024–3029.
33 S. Plantman, M. Patarroyo, K. Fried, A. Domogatskaya, K. Tryggvason, H. Hammarberg and S. Cullheim, *Mol. Cell. Neurosci.*, 2008, **39**, 50–62.

34 E. S. Rosenzweig, G. Courtine, D. L. Jindrich, J. H. Brock, A. R. Ferguson, S. C. Strand, Y. S. Nout, R. R. Roy, D. M. Miller, M. S. Beattie, L. A. Havton, J. C. Bresnahan, V. R. Edgerton and M. H. Tuszynski, *Nat. Neurosci.*, 2010, **13**, 1505–1510.

35 O. Raineteau and M. E. Schwab, *Nat. Rev. Neurosci.*, 2001, **2**, 263–273.

36 X. Li, Y. Zhao, S. Cheng, S. Han, M. Shu, B. Chen, X. Chen, F. Tang, N. Wang, Y. Tu, B. Wang, Z. Xiao, S. Zhang and J. Dai, *Biomaterials*, 2017, **137**, 73–86.

37 E. D. Wirth 3rd, P. J. Reier, R. G. Fessler, F. J. Thompson, B. Uthman, A. Behrman, J. Beard, C. J. Vierck and D. K. Anderson, *J. Neurotrauma*, 2001, **18**, 911–929.

38 N. A. Silva, N. Sousa, R. L. Reis and A. J. Salgado, *Prog. Neurobiol.*, 2014, **114**, 25–57.

39 P. Assinck, G. J. Duncan, B. J. Hilton and J. R. Plemel, *Nat. Neurosci.*, 2017, **20**, 637–647.

40 M. V. Sofroniew, *Nature*, 2018, **557**, 343–350.

41 B. Shrestha, K. Coykendall, Y. Li, A. Moon, P. Priyadarshani and L. Yao, *Stem Cell Res. Ther.*, 2014, **5**, 91.

42 H. Babaloo, S. Ebrahimi-Barough, M. A. Derakhshan, M. Yazdankhah, N. Lotfibakhshaiesh, M. Soleimani, M. T. Joghataei and J. Ai, *J. Cell Physiol.*, 2019, **234**, 11060–11069.

43 S. Pan, Z. Qi, Q. Li, Y. Ma, C. Fu, S. Zheng, W. Kong, Q. Liu and X. Yang, *Artif. Cells, Nanomed., Biotechnol.*, 2019, **47**, 651–664.

44 J. Yuan, M. Zou, X. Xiang, H. Zhu, W. Chu, W. Liu, F. Chen and J. Lin, *J. Surg. Res.*, 2015, **195**, 235–245.

45 F. Boato, S. Hendrix, S. C. Huelsenbeck, F. Hofmann, G. Grosse, S. Djalali, L. Klimaschewski, M. Auer, I. Just, G. Ahnert-Hilger and M. Holtje, *J. Cell Sci.*, 2010, **123**, 1652–1662.

46 D. M. Basso, M. S. Beattie and J. C. Bresnahan, *J. Neurotrauma*, 1995, **12**, 1–21.